

Search for Lorentz-invariance violation with the first KATRIN data

M. Aker,¹ D. Batzler,¹ A. Beglarian,² J. Behrens,¹ A. Berlev,³ U. Besserer,¹ B. Bieringer,⁴ F. Block,⁵ S. Bobien,⁶ B. Bornschein,¹ L. Bornschein,¹ M. Böttcher,⁴ T. Brunst,^{7,8} T. S. Caldwell,^{9,10} R. M. D. Carney,¹¹ S. Chilingaryan,² W. Choi,⁵ K. Debowski,¹² M. Descher,⁵ D. Díaz Barrero,¹³ P. J. Doe,¹⁴ O. Dragoun,¹⁵ G. Drexlin,⁵ F. Edzards,^{7,8} K. Eitel,¹ E. Ellinger,¹² R. Engel,¹ S. Enomoto,¹⁴ A. Felden,¹ J. A. Formaggio,¹⁶ F. M. Fränkle,¹ G. B. Franklin,¹⁷ F. Friedel,¹ A. Fulst,⁴ K. Gauda,⁴ A. S. Gavin,^{9,10} W. Gil,¹ F. Glück,¹ R. Grössle,¹ R. Gumbsheimer,¹ V. Hannen,⁴ N. Haußmann,¹² K. Helbing,¹² S. Hickford,¹ R. Hiller,¹ D. Hillesheimer,¹ D. Hinz,¹ T. Höhn,¹ T. Houdy,^{7,8} A. Huber,¹ A. Jansen,¹ C. Karl,^{7,8} J. Kellerer,⁵ M. Kleifges,² M. Klein,¹ C. Köhler,^{7,8} L. Köllenberger,¹ A. Kopmann,² M. Korzeczek,⁵ A. Kovalík,¹⁵ B. Krasch,¹ H. Krause,¹ L. La Cascio,⁵ T. Lasserre,¹⁸ T. L. Le,¹ O. Lebeda,¹⁵ B. Lehnert,¹¹ A. Lokhov,⁴ M. Machatschek,¹ E. Malcherek,¹ M. Mark,¹ A. Marsteller,¹ E. L. Martin,^{9,10} C. Melzer,¹ S. Mertens,^{7,8,*} J. Mostafa,² K. Müller,¹ H. Neumann,⁶ S. Niemes,¹ P. Oelpmann,⁴ D. S. Parno,¹⁷ A. W. P. Poon,¹¹ J. M. L. Poyato,¹³ F. Priester,¹ J. Ráliš,¹⁵ S. Ramachandran,¹² R. G. H. Robertson,¹⁴ W. Rodejohann,¹⁹ C. Rodenbeck,⁴ M. Röllig,¹ C. Röttele,¹ M. Ryšavý,¹⁵ R. Sack,^{1,4} A. Saenz,²⁰ R. Salomon,⁴ P. Schäfer,¹ L. Schimpf,^{4,5} M. Schlösser,¹ K. Schlösser,¹ L. Schlüter,^{7,8} S. Schneidewind,⁴ M. Schrank,¹ A. Schwemmer,^{7,8} M. Šefčík,¹⁵ V. Sibille,¹⁶ D. Siegmann,^{7,8} M. Slezák,^{7,8} F. Spanier,²¹ M. Steidl,¹ M. Sturm,¹ H. H. Telle,¹³ L. A. Thorne,²² T. Thümmel,¹ N. Titov,³ I. Tkachev,³ K. Urban,^{7,8} K. Valerius,¹ D. Vénos,¹⁵ A. P. Vizcaya Hernández,¹⁷ C. Weinheimer,⁴ S. Welte,¹ J. Wendel,¹ M. Wetter,⁵ J. Wickles,^{8,23,†} C. Wiesinger,^{7,8} J. F. Wilkerson,^{9,10} J. Wolf,⁵ S. Wüstling,² J. Wydra,¹ W. Xu,¹⁶ S. Zadoroghny,³ and G. Zeller¹

(KATRIN Collaboration)

¹*Institute for Astroparticle Physics (IAP), Karlsruhe Institute of Technology (KIT),
Hermann-von-Helmholtz-Platz 1, 76344 Eggenstein-Leopoldshafen, Germany*

²*Institute for Data Processing and Electronics (IPE), Karlsruhe Institute of Technology (KIT),
Hermann-von-Helmholtz-Platz 1, 76344 Eggenstein-Leopoldshafen, Germany*

³*Institute for Nuclear Research of Russian Academy of Sciences, 60th October Anniversary Prospect 7a,
117312 Moscow, Russia*

⁴*Institute for Nuclear Physics, University of Münster, Wilhelm-Klemm-Str. 9, 48149 Münster, Germany*

⁵*Institute of Experimental Particle Physics (ETP), Karlsruhe Institute of Technology (KIT),
Wolfgang-Gaede-Str. 1, 76131 Karlsruhe, Germany*

⁶*Institute for Technical Physics (ITEP), Karlsruhe Institute of Technology (KIT),
Hermann-von-Helmholtz-Platz 1, 76344 Eggenstein-Leopoldshafen, Germany*

⁷*Technische Universität München, James-Frank-Str. 1, 85748 Garching, Germany*

⁸*Max-Planck-Institut für Physik, Föhringer Ring 6, 80805 München, Germany*

⁹*Department of Physics and Astronomy, University of North Carolina,
Chapel Hill, North Carolina 27599, USA*

¹⁰*Triangle Universities Nuclear Laboratory, Durham, North Carolina 27708, USA*

¹¹*Institute for Nuclear and Particle Astrophysics and Nuclear Science Division,
Lawrence Berkeley National Laboratory, Berkeley, California 94720, USA*

¹²*Department of Physics, Faculty of Mathematics and Natural Sciences, University of Wuppertal,
Gaußstraße 20, 42119 Wuppertal, Germany*

¹³*Departamento de Química Física Aplicada, Universidad Autonoma de Madrid,
Campus de Cantoblanco, 28049 Madrid, Spain*

¹⁴*Center for Experimental Nuclear Physics and Astrophysics, and Department of Physics,
University of Washington, Seattle, Washington 98195, USA*

¹⁵*Nuclear Physics Institute, Czech Academy of Sciences, 25068 Řež, Czech Republic*

¹⁶*Laboratory for Nuclear Science, Massachusetts Institute of Technology,
77 Massachusetts Ave, Cambridge, Massachusetts 02139, USA*

¹⁷*Department of Physics, Carnegie Mellon University, Pittsburgh, Pennsylvania 15213, USA*

¹⁸*IRFU (DPhP & APC), CEA, Université Paris-Saclay, 91191 Gif-sur-Yvette, France*

¹⁹*Max-Planck-Institut für Kernphysik, Saupfercheckweg 1, 69117 Heidelberg, Germany*

²⁰*Institut für Physik, Humboldt-Universität zu Berlin, Newtonstraße 15, 12489 Berlin, Germany*

²¹*Institute for Theoretical Astrophysics, University of Heidelberg, Albert-Ueberle-Straße 2,
69120 Heidelberg, Germany*

²²*Institut für Physik, Johannes-Gutenberg-Universität Mainz, 55099 Mainz, Germany*²³*Ludwig-Maximilians-Universität München, Geschwister-Scholl-Platz 1, 80539 München, Germany*
 (Received 2 October 2022; revised 8 February 2023; accepted 14 March 2023; published 26 April 2023)

Some extensions of the Standard Model of particle physics allow for Lorentz invariance and charge-parity-time invariance violations. In the neutrino sector strong constraints have been set by neutrino-oscillation and time-of-flight experiments. However, some Lorentz-invariance-violating parameters are not accessible via these probes. In this work, we focus on the parameters $(a_{\text{of}}^{(3)})_{00}$, $(a_{\text{of}}^{(3)})_{10}$, and $(a_{\text{of}}^{(3)})_{11}$ which would manifest themselves in a nonisotropic β -decaying source as a sidereal oscillation and an overall shift of the spectral endpoint. Based on the data of the first scientific run of the KATRIN experiment, we set the first 90% confidence-level limit on $|(a_{\text{of}}^{(3)})_{11}|$ of $<0.9 \times 10^{-6}$ GeV to 3.7×10^{-6} GeV, depending on the phase. Moreover, we derive new constraints on $(a_{\text{of}}^{(3)})_{00}$ and $(a_{\text{of}}^{(3)})_{10}$.

DOI: 10.1103/PhysRevD.107.082005

I. INTRODUCTION

Charge-parity-time (*CPT*) and Lorentz invariance are central ingredients of modern physics and of the Standard Model (SM) of particle physics. However, some extensions of the SM such as string theories [1,2], loop quantum gravity [3], and noncommutative quantum field theories [4] suggest that *CPT* and Lorentz invariance may be violated at high energies. Yet, so far, no experimental evidence for *CPT* or Lorentz invariance violation was ever observed and the parameter space is strongly constrained.

Deviations from Lorentz symmetry are typically described in a relativistic effective field theory, the so-called Standard Model extension (SME) [5–7]. In particular, the SME specifies all possible Lorentz-invariance-violating operators for neutrino propagation, many of which have been constrained with neutrino-oscillation experiments [8–17]. The so-called “oscillation-free” (of) modes, which cannot be assessed via oscillation experiments, are usually constrained by time-of-flight experiments, which probe the neutrinos’ group velocity compared to that of photons. However, there are four oscillation-free parameters, $(a_{\text{of}}^{(d=3)})_{jm}$, where j and m denote the angular momentum quantum numbers with $j = 0, 1$, $m = -1, 0, 1$, and d stands for the mass dimension. These parameters can only be accessed by interaction processes, such as the β decay of tritium [18,19].

The operators arise from the introduction of the Lorentz-invariance-violating four-vector a^μ , which can be illustrated as an external vector field, as shown in Fig. 1. Lorentz invariance violation of type a^μ in tritium beta decay is governed by Lagrangian contributions for each of the fermions

$$L_{\text{SME}}^a = -\bar{\psi}_w a^\mu \gamma_\mu \psi_w, \quad (1)$$

* Corresponding author.
susanne.mertens@tum.de

† Corresponding author.
johannes.wickles@mail.de

where the species subscript $w \in \{\text{T, He, e, n}\}$ labels the tritium, helium, electron, and neutrino, respectively. In the calculation of the β -decay spectrum, the momenta of the external particles are modified by a^μ and, at first order, terms $\propto a^\mu p_\mu = a^0 p_0 - \vec{a} \cdot \vec{p}$ appear, where p_μ denotes the momentum of the emitted electron. This term causes both a time-dependent and time-independent shift of the spectral endpoint E_0 . The former only occurs for nonisotropic β sources, where $\vec{a} \cdot \vec{p}$ does not vanish. The time dependence is caused by the rotation of the Earth in the vector field a^μ , which leads to a temporal change of the relative direction between the electron’s momentum and the vector field and hence results in a periodic change of the endpoint with sidereal frequency $\omega_\oplus = \frac{2\pi}{23\text{h}56\text{min}}$. The latter is caused by the

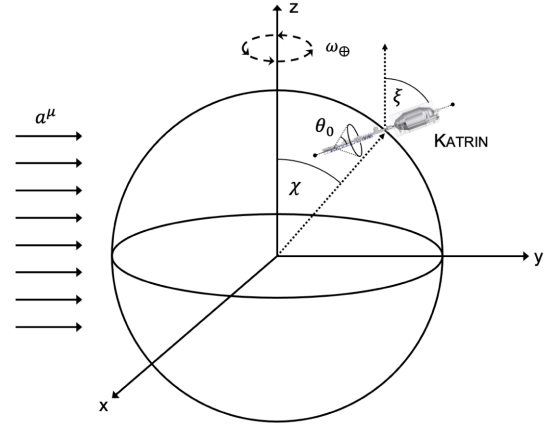


FIG. 1. Sketch of the equatorial coordinate system. The Earth is rotating with ω_\oplus within the Lorentz-invariance-violating vector field a^μ , defined to be perpendicular to the z axis. Therefore, the KATRIN experiment, which is located at the colatitude $\chi \approx 41^\circ$, is moving with velocity β_{rot} (rotation velocity of the Earth at the position of KATRIN). The beam axis of the KATRIN experiment is tilted with respect to the local north by $\xi \approx 17^\circ$ (this angle is enlarged in the figure for illustration purposes). The angle $\theta_0 \approx 50.4^\circ$ depicts the experimental acceptance angle with respect to the KATRIN beam axis.

isotropic part a^0 as well as the component a^z along the rotation axis. Usually the operator a^μ is expressed in spherical decomposition, where the isotropic part is represented by $(a_{\text{of}}^{(3)})_{00}$, the part along the rotation axis by $(a_{\text{of}}^{(3)})_{10}$, and the periodically time-dependent part by $(a_{\text{of}}^{(3)})_{11}$ and $(a_{\text{of}}^{(3)})_{1-1} = -(a_{\text{of}}^{(3)})_{11}^*$ [18,19].

$$\begin{aligned} \Delta E_0 = & (\gamma - \beta_{\text{rot}} B \sin \xi) \frac{1}{\sqrt{4\pi}} (a_{\text{of}}^{(3)})_{00} + \sqrt{\frac{3}{4\pi}} B \sin \chi \cos \xi (a_{\text{of}}^{(3)})_{10} + \sqrt{\frac{3}{2\pi}} \cos(\omega_{\oplus} t) [(\beta_{\text{rot}} - B \sin \xi) \text{Im}((a_{\text{of}}^{(3)})_{11}) \\ & - B \cos \xi \cos \chi \text{Re}((a_{\text{of}}^{(3)})_{11})] + \sqrt{\frac{3}{2\pi}} \sin(\omega_{\oplus} t) [(\beta_{\text{rot}} - B \sin \xi) \text{Re}((a_{\text{of}}^{(3)})_{11}) + B \cos \xi \cos \chi \text{Im}((a_{\text{of}}^{(3)})_{11})], \end{aligned} \quad (2)$$

where γ is the Lorentz factor, β_{rot} is the rotation velocity of Earth at the location of the experiment, χ is the colatitude of the experiment, and ξ is the orientation of the experimental beam axis with respect to the local north, as shown in Fig. 2. The factor $B = M_T^{-1} (2\pi(1 - \cos \theta_0))^{-1} \pi \sqrt{E_{\text{tot}}^2 - m_e^2} \sin^2 \theta_0$ depends on the mass of the tritium atom M_T , the mass of the electron m_e , the total electron energy without Lorentz invariance violation E_{tot} , and the acceptance angle θ_0 , which is illustrated in Fig. 2. From this it becomes clear that an acceptance angle of less than 90° , and thus an anisotropy, is necessary to cause a temporal oscillation in addition to a time-independent shift.

In this work we use data from the first scientific run of the Karlsruhe Tritium Neutrino (KATRIN) experiment, which took place in spring 2019 and lasted about one month. The data was acquired in 361 two-hour-long scans, from each of which the spectral endpoint E_0 was inferred individually. This time series of E_0 measurements is used to

In this work, we assume an isotropic tritium β -decay source and introduce anisotropy by considering a subset of β electrons, which are emitted under a conical solid angle, defined by the experimental acceptance angle θ_0 . The endpoint E_0 of their energy spectrum is modified by a^μ in the following way:

search for a temporal oscillation, expressed by $\Delta E_0 = A \cos(\omega_{\oplus} t - \phi)$, where the oscillation is described by an amplitude A and phase ϕ and t refers to the standard solar time. The amplitude can directly be used to limit the Lorentz-invariance-violating parameter $(a_{\text{of}}^{(3)})_{11}$. By considering the oscillatory parts, $a \cdot \sin(\omega_{\oplus} t)$ and $b \cdot \cos(\omega_{\oplus} t)$, of Eq. (2), we can write

$$\begin{aligned} A = & \sqrt{a^2 + b^2} \\ = & \sqrt{\frac{3}{2\pi}} |(a_{\text{of}}^{(3)})_{11}| \sqrt{B^2 \cos^2 \chi \cos^2 \xi + (\beta_{\text{rot}} - B \sin \xi)^2}. \end{aligned} \quad (3)$$

II. KATRIN EXPERIMENT

The goal of KATRIN is to measure the effective electron antineutrino mass m_ν with a sensitivity of <0.3 eV at 90% confidence level (CL) after about 1000 days of taking

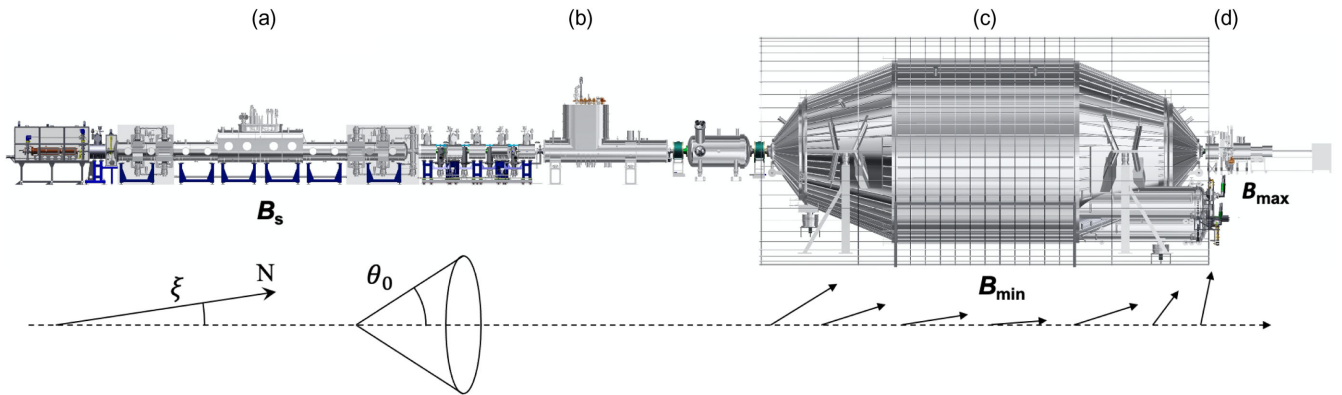


FIG. 2. Main components of the KATRIN experiment: (a) Tritium source, (b) transport and pumping sections, (c) main spectrometer, (d) focal plane detector. The dashed line below illustrates the KATRIN beamline. The experiment has an orientation of $\xi \approx 16^\circ$ east to the local north N. The acceptance angle $\theta_0 = 50.4^\circ$ defines the acceptance cone of the β electrons. The black arrows below the spectrometer indicate the electron momentum (without electric field). When propagating from B_s to B_{min} , the pitch angle θ (angle between the electron momentum and the magnetic field lines) is reduced; while when moving from B_s to B_{max} , the pitch angle is increased. An electron starting with $\theta > \theta_0$ will be reflected at B_{max} .

data [20,21]. Recently, KATRIN has published the first direct sub-eV upper limit on the neutrino mass of $m_\nu < 0.8$ eV (90% CL) based on the first two data-taking campaigns [22]. The experiment will continue taking data for another few years.

KATRIN combines a high-luminosity windowless gaseous molecular tritium source with a high-resolution spectrometer based on the principle of magnetic adiabatic collimation with electrostatic filtering (MAC-E filter) [23,24]. This combination allows us to perform a precise integral measurement of the tritium β -decay spectrum in the close vicinity of the spectral endpoint $E_0 \approx 18.6$ keV, where the impact of the neutrino mass is maximal.

Technically this is realized by a 70-m long experimental beamline, shown in Fig. 2, which is located at the Karlsruhe Institute of Technology (KIT) in Germany. The gaseous tritium source (a) is part of a closed tritium loop [25], which provides up to 10^{11} β decays per second in the 10 m-long, 90 mm-diameter source beam tube. The resulting β electrons are guided by a system of superconducting magnets towards the spectrometer section [26]. In the transport section (b), connecting the source and spectrometer, neutral and ionized tritium is removed by a differential and cryogenic pumping system [27]. The main spectrometer (c) analyzes the kinetic energy of the β electrons with the MAC-E-filter technique. Essentially, it acts as an electrostatic filter, allowing only β electrons with sufficient kinetic energy to overcome its precisely adjustable retarding potential U [28]. In addition, a slowly decreasing magnetic field (from $B_{\max} = 4.24$ T to $B_{\min} = 0.63$ mT in the center of the main spectrometer) aligns the momenta of the isotropically created electrons. This magnetic adiabatic collimation provides a large angular acceptance ($\theta_0 = 50.4^\circ$) with a sharp cutoff energy [$\Delta E(18.6 \text{ keV}) = 2.8$ eV] at the same time. By measuring the rate of transmitted electrons (charge $q = -e$) as a function of the retarding energy qU the integral β -decay spectrum is obtained, as illustrated in Fig. 3(a). The electrons are detected by a 148-pixel silicon PIN focal-plane detector (d), installed at the exit of the spectrometer [29].

For the presented analysis it is important that the KATRIN experiment accepts only electrons that are emitted at an angle of less than 50.4° relative to the magnetic field lines in the source. The acceptance angle $\theta_0 = \arcsin(\sqrt{B_s/B_{\max}})$ is determined by the source magnetic field $B_s = 2.52$ T and the maximal magnetic field in the beamline $B_{\max} = 4.24$ T. These values are chosen to exclude electrons with a long path through the source and hence increased scattering probability. It is this selection of direction which makes KATRIN sensitive to the anisotropic Lorentz-invariance-violating operator $(a_{\text{of}}^{(3)})_{11}$.

This work uses data from the first high-luminosity (2.45×10^{10} Bq) tritium campaign, which ran from April 10 to May 13, 2019 [30,31]. The integral spectrum was recorded by repeatedly scanning the energy interval from $E_0 - 90$ eV to $E_0 + 50$ eV. In each so-called scan a series of 39 nonequidistant high-voltage (HV) set points

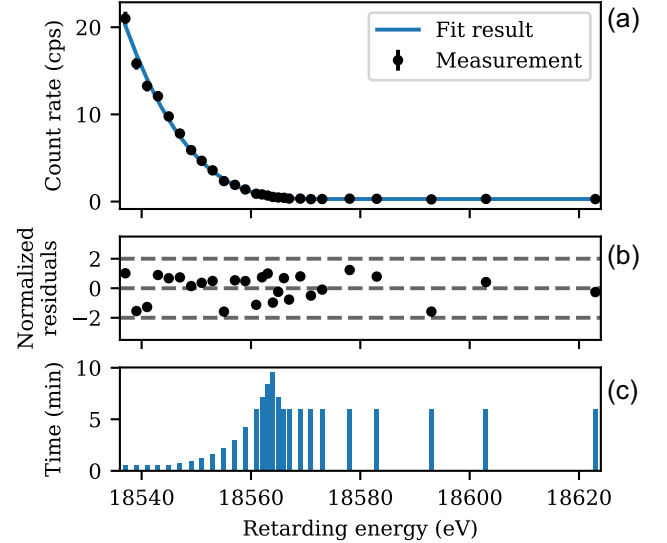


FIG. 3. (a) Electron spectrum $R(qU)$ of a single scan where all pixels are combined (uniform fit). The spectrum of the best fit $R_{\text{calc}}(qU)$ extends to the endpoint E_0 and lies on top of an energy-independent background R_{bg} . (b) Residuals of $R(qU)$ relative to the 1σ -uncertainty band of the best fit model. (c) Measurement-time distribution.

is applied to the main spectrometer. The HV set points U are applied in alternating upward (up-scan) and downward (down-scan) directions to compensate for possible time-dependent drifts of the system to first order. The measurement time at each HV set point lasts between 17 and 576 s, as shown in Fig. 3(c). The net scan time is about 2 hours.

The presented search for Lorentz invariance violation follows the same initial protocol as the neutrino-mass analysis. To this end, we choose an analysis interval covering a region from 40 eV below E_0 (22 HV set points) to 50 eV above E_0 (5 HV set points). In the same manner as for the neutrino-mass analysis, we apply quality cuts to each scan and select 274 stable scans. The 117 selected pixels (79% of the detector area) are combined to one effective pixel (so-called uniform fit), which leads to 274 integral spectra $R(qU_i)$ with about 7400 events each. For the neutrino-mass analysis, these are further combined to a single high-statistics scan, while in this work they are analyzed individually to access the temporal variation of the spectral endpoint.

III. ENDPOINT FIT OF INTEGRAL SPECTRUM

The theoretical spectrum $R_{\text{calc}}(qU)$ consists of the differential β spectrum R_β , the experimental response function $f(E, qU)$, and a retarding-energy-independent background R_{Bg} :

$$R_{\text{calc}}(qU) = A_s \cdot N_T \int R_\beta(E; m_\nu^2, E_0) \cdot f(E - qU) dE + R_{\text{Bg}} \quad (4)$$

where A_s is the amplitude of the signal and N_T is the effective number of tritium atoms in the source. E denotes the energy of the electron. The differential spectrum, described in detail, for example, in [31,32], depends on the endpoint of the tritium spectrum E_0 as well as the effective electron antineutrino mass $m_\nu^2 = \sum_{i=1}^3 |U_{ei}|^2 m_i^2$, where U is the PNMS matrix and m_i the masses of the neutrino-mass eigenstates. In addition, it is considered that the tritium molecule can be in rotational, vibrational, and electronic excited states, which are described by means of a final-states distribution. The response function $f(E, qU)$ describes the transmission probability of an electron as a function of its energy. It includes the spectrometer resolution and energy losses due to scattering in the gaseous source.

The computed spectrum \vec{R}_{calc} is fit to the data \vec{R}_{data} by minimizing

$$\chi^2(\vec{\eta}) = (\vec{R}_{\text{calc}}(\vec{\eta}) - \vec{R}_{\text{data}})^T C^{-1} (\vec{R}_{\text{calc}}(\vec{\eta}) - \vec{R}_{\text{data}}), \quad (5)$$

with respect to the free parameters $\vec{\eta}$. For the neutrino-mass analysis [31] the combined data of all scans are analyzed with the four free fit parameters A_s , E_0 , R_{bg} , and m_ν^2 . An excellent agreement of the model with the data was demonstrated in [30,31]. In this work, in contrast, we analyze the scans separately, which leads to an individual endpoint for each scan. Moreover, we set m_ν^2 to zero in the fits, since we assume it to be a time-independent parameter, which has no effect on the oscillation signal due to Lorentz invariance violation. An example fit can be seen in Fig. 3(a).

Every fitted endpoint has an uncertainty, which is composed of a statistical and a systematic part. As we are interested in a temporal variation of the endpoint, only the statistical uncertainties and those systematic uncertainties, which can vary with time, are of concern for this analysis. For example, the time-independent uncertainty on the theoretical description of the molecular final states would have the same effect on the endpoints of all scans, and thus would not affect the oscillation signal. In contrast, the magnetic field may vary slightly from scan to scan and therefore influences the uncertainty of the fitted oscillation of the endpoint.

Uncertainties of a statistical nature, such as the Poisson uncertainty of each data point and additional source activity and background fluctuations, are included via the covariance matrix C of Eq. (5). In particular, a background component, present during this measurement campaign, which arises from ^{219}Rn and ^{220}Rn decays inside of the main spectrometer, leads to a non-Poissonian (NP) overdispersion of the rate [30,31,33]. To determine the influence of systematic uncertainties we employ the Monte-Carlo propagation technique [31]. Here, the data are fitted about 10^5 times while varying the relevant systematic parameters (e.g., the magnetic fields and source properties) in each fit. The distribution of fitted endpoints is used to determine the best-fit value and uncertainty of the endpoint.

TABLE I. 1σ uncertainties on the endpoint E_0 in eV for a fit to a Monte-Carlo-generated spectrum of a single scan. The values are calculated using Monte-Carlo propagation.

Effect	$\sigma(E_0)$
Non-Poissonian background	0.069
Subrun activity fluctuation	0.006
Source electric potential	0.005
Column density ρd	0.004
Magnetic fields	0.004
Isotopologue concentration	<0.001
Total syst. uncertainties	0.070
Stat. uncertainty	0.247
Total uncertainty	0.257

The statistical uncertainty of the endpoint in a single scan is $\sigma_{E_0}^{\text{stat}} = 247$ meV, which dominates over the total systematic uncertainty of $\sigma_{E_0}^{\text{syst}} = 70$ meV. The largest effect beyond the statistical uncertainty arises from the above-mentioned non-Poissonian background component. This overdispersion of the background-rate distribution increases the statistical uncertainty and contributes 69 meV to the uncertainty budget of the endpoint in each scan. Uncertainties of the column density ρd (the integral of the gas density ρ over the length of the source d), activity fluctuations during a scan, the concentration of different tritium isotopologues in the source, the source electric potential, as well as the magnetic field stability, contribute with less than 10 meV each to the endpoint uncertainty per scan. All uncertainties are summarized in Table I.

Since we are interested in a temporal oscillation of the endpoint, we verified the absence of any oscillatory behavior of the individual slow control and nuisance parameters. We exclude any statistically significant sinusoidal time evolution of the background rate, the source activity, and any of the systematic parameters mentioned above.

The spectral model $R_{\text{calc}}(qU)$ assumes a constant endpoint, and thus neglects the fact that, in the case of Lorentz invariance violation, the endpoint would slightly change during the course of a 2-hour scan. We justify this approximation, by introducing an effective time, as illustrated in Fig. 4. To this end, we simulate several up and down scans, including a continuously changing endpoint, according to various assumed values of Lorentz invariance violation. We fit these simulated scans with the theoretical model $R_{\text{calc}}(qU)$ and demonstrate that the inferred endpoint agrees to within <1% with the theoretical true endpoint at a fixed effective time t_e relative to the start of the 2-hour scan. As the different HV set points have different sensitivity to the endpoint, t_e depends on the measurement-time distribution and the scan direction. We find $t_e = t_0 + 87$ min (for up scans) and $t_e = t_0 + 52$ min (for down scans), where t_0 is the start time of the scan.

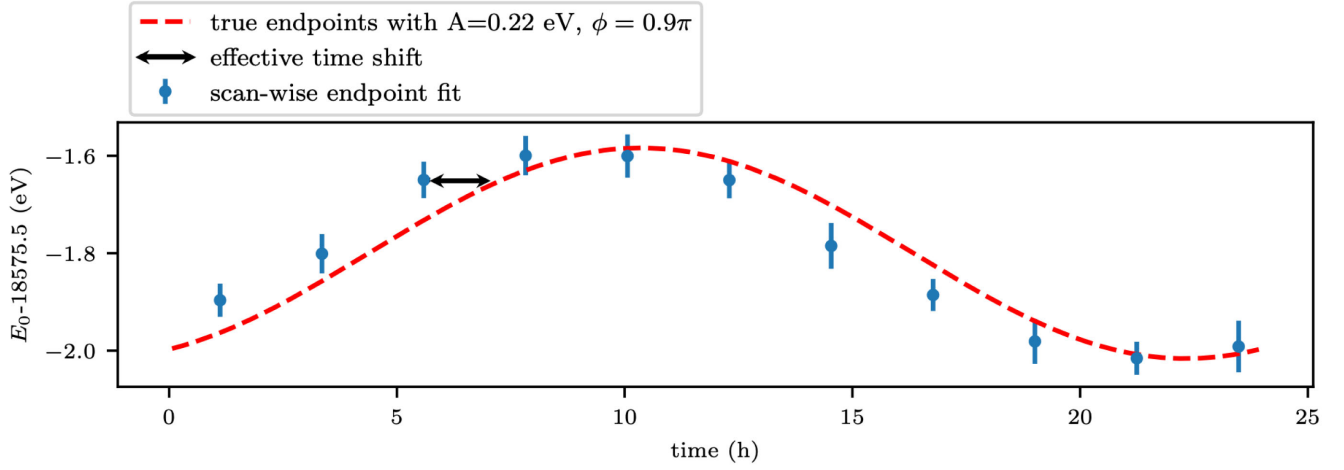


FIG. 4. Illustration of the effective-time concept. Here we assume a certain Lorentz-invariance-violation scenario, illustrated by the red line. The corresponding individual endpoint measurements (blue dots) are shown at the time of the start of each 2-hour scan. Shifting the data points by a fixed time (here: 87 minutes) reproduces the true variation of the endpoint. An individual time shift is evaluated for up scans and down scans (see main text). To good approximation the time shift is independent of the size of the Lorentz invariance violation.

IV. SEARCH FOR SIDEREAL ENDPOINT OSCILLATION

The fitted endpoints with corresponding uncertainties of the individual scans, illustrated in Fig. 5, can be used to search for oscillations with sidereal frequency $\omega_{\oplus} \approx 2\pi / (23 \text{ h } 56 \text{ min})$ caused by the Lorentz-invariance-violating

parameter $(a_{\text{of}}^{(3)})_{11}$. The oscillation is described by $E_0 = D + A \cos(\omega_{\oplus} t - \phi)$ with the baseline D , the amplitude A and the phase ϕ , which are treated as free parameters.

To set a limit on the amplitude and phase, we used a two-dimensional χ^2 -grid search in (A, ϕ) . At each grid point the amplitude A and the phase ϕ are fixed parameters, while we

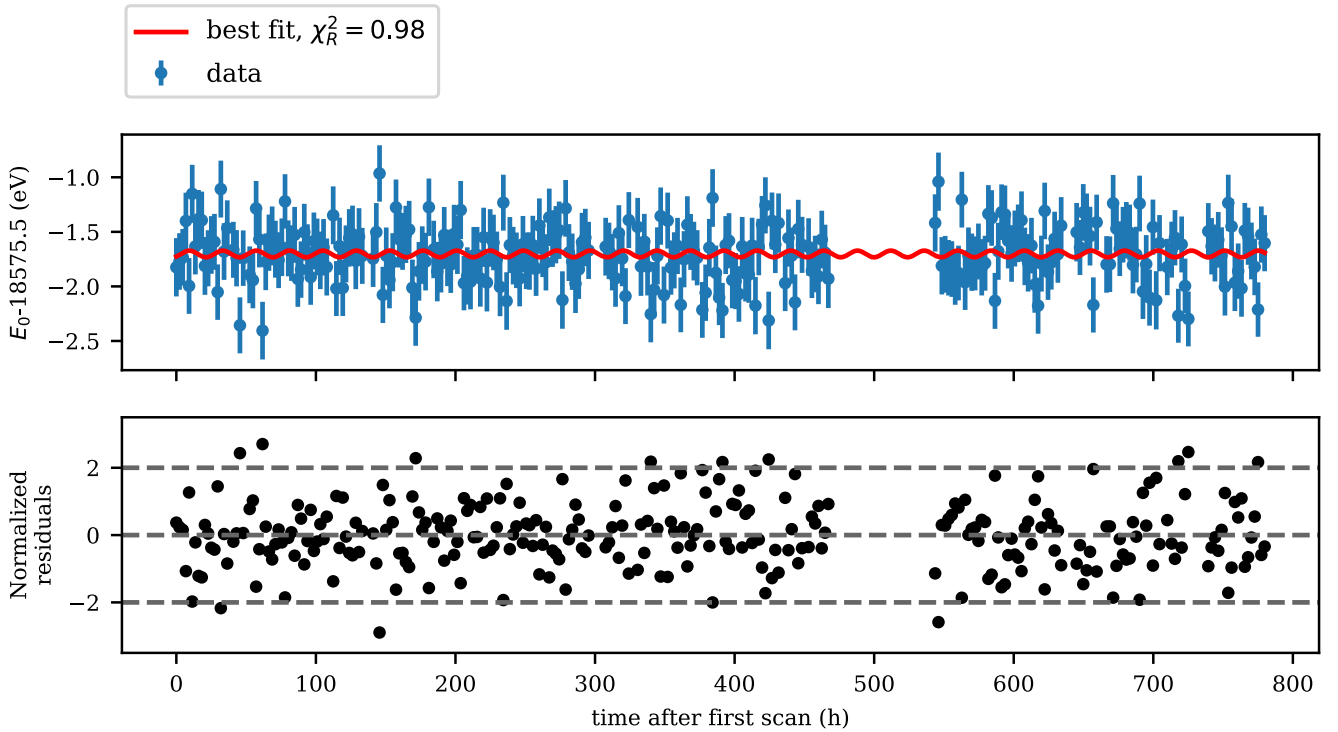


FIG. 5. Illustration of the fitted endpoints (blue dots) at their effective times t_e . The red line shows the best fit of an oscillation with sidereal frequency and free amplitude and free phase. The best fit corresponds to $A_{\text{best}} \approx 0.03 \text{ eV}$ and $\phi_{\text{best}} \approx 0.78\pi$ and has a reduced $\chi_R^2 = 0.98$. The bottom panel displays the normalized residuals of the data fit (black).

treat the baseline D as a free parameter. An exclusion contour is extracted from the χ^2 map using a likelihood ratio as test statistic $\Lambda(A, \phi) = \frac{\mathcal{L}(A, \phi)}{\mathcal{L}_{\text{best}}}$. Applying Wilks' theorem, $\Delta\chi^2 \equiv -2 \ln \Lambda(A, \phi) = \chi^2(A, \phi) - \chi^2_{\text{best}}$ behaves according to a χ^2 distribution with 2 degrees of freedom [34]. This means that for a confidence level of 90%, one excludes all grid points for which $\Delta\chi^2 > \chi^2_c \approx 4.61$ holds. We confirmed the correct coverage of this approach by means of Monte-Carlo simulations. For about 5000 simulations of the experiment, including both statistical and systematic uncertainties, and assuming the null hypothesis H_0 ($A = 0$ eV) as well as several alternative hypotheses H_1 ($A \neq 0$ eV), we show that the $\Delta\chi^2$ distribution follows the theoretical χ^2 curve and gives a critical χ^2 of $\chi^2_c = 4.55 \pm 0.06$, which is in good agreement with Wilks' theorem. Finally, according to Eq. (3) we translate the limit on the amplitude A into a limit on $(a_{\text{of}}^{(3)})_{11}$.

V. RESULTS

In order to prevent human-induced bias in the analysis and to determine a sensitivity of the considered dataset to possible Lorentz invariance violation, the χ^2 grid scan is first performed on simulated data, assuming no Lorentz invariance violation. The sensitivity to the amplitude of the sidereal oscillation is found to be $A < 0.05$ eV (90% CL). This translates into a sensitivity of $|(a_{\text{of}}^{(3)})_{11}| < 2.3 \times 10^{-6}$ GeV (90% CL) by means of Eq. (3).

After the investigation with simulated data, a grid search is performed with the real data, as shown in Fig. 6. The best

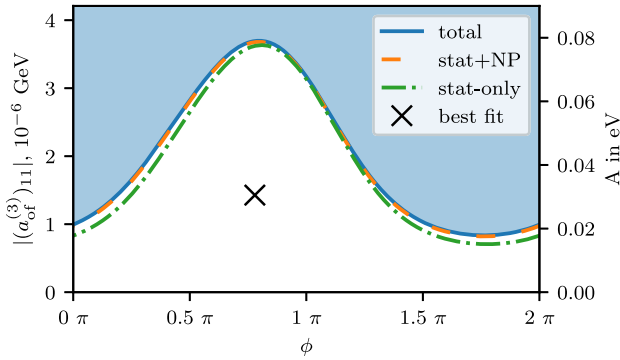


FIG. 6. 90% CL exclusion limit for the Lorentz-invariance-violating parameter $|(a_{\text{of}}^{(3)})_{11}|$ and the phase ϕ . The right y axis displays the corresponding amplitude of the endpoint oscillation, according to Eq. (3). Using a χ^2 -grid search and Wilks' theorem, the exclusion limit for the total uncertainties (blue solid line) are calculated. The green dashed-dotted line shows the exclusion limit, including only the statistical uncertainty. The orange dashed line includes an enlarged statistical uncertainty due to the non-Poissonian (NP) distribution of the background rate, as explained in the main text. The best fit is shown by the black cross.

fit is found at $|(a_{\text{of}}^{(3)})_{11}|_{\text{best}} = 1.4 \times 10^{-6}$ GeV (corresponding to $A_{\text{best}} = 0.03$ eV) and $\phi_{\text{best}} = 0.78\pi$. The difference of the χ^2 of the null hypothesis and the best fit is $\Delta\chi^2 = 1.86$, which corresponds (for 2 degrees of freedom) to a p value of 0.39 and is thus not significant at 90% confidence level. The resulting 90% confidence-level exclusion curve is illustrated by the shaded region in Fig. 6. The strongest exclusion of $|(a_{\text{of}}^{(3)})_{11}| < 1 \times 10^{-6}$ GeV ($A < 0.02$ eV) is found at a phase of $\phi \approx 0\pi$.

In addition we can also constrain $(a_{\text{of}}^{(3)})_{00}$ and $(a_{\text{of}}^{(3)})_{10}$ as done in [18], by searching for a time-independent shift of the Q value of the β decay with respect to the theoretical Q value. In order to assess the Q value in KATRIN the measured effective endpoint E_0 has to be corrected for the electric potential in the source Φ_{so} , the work function of the spectrometer Φ_{sp} and the molecular recoil energy E_{rec} , which leads to $Q^{\text{KATRIN}} = E_0 + E_{\text{rec}} - (\Phi_{\text{so}} - \Phi_{\text{sp}})$. For this analysis, E_0 is obtained from a fit to the combined data of all scans; see [31] for details.

The calculated Q value Q^{calc} is given by a high-precision measurement of the mass difference of ${}^3\text{He}$ and T [35], corrected for molecular dissociation and ionization energies [36]. A significant difference between the Q^{KATRIN} and Q^{calc} could be interpreted as a signature of Lorentz invariance violation, caused by the parameters $(a_{\text{of}}^{(3)})_{00}$ and $(a_{\text{of}}^{(3)})_{10}$ [see Eq. (2)].

In order to disentangle both parameters, one needs to make use of a second experiment, for example, the Mainz direct neutrino-mass experiment [37], which is located at a different site ($\chi = 40^\circ, \xi = -65^\circ$) from KATRIN ($\chi = 41^\circ, \xi = 16^\circ$). We infer both parameters by setting up a system of two linear equations, derived from Eq. (2),

$$\Delta E_0^{\text{K(M)}} = \Delta Q^{\text{K(M)}} = \gamma \frac{1}{\sqrt{4\pi}} (a_{\text{of}}^{(3)})_{00} - \sqrt{\frac{3}{4\pi}} B^{\text{K(M)}} \sin \chi^{\text{K(M)}} \cos \xi^{\text{K(M)}} (a_{\text{of}}^{(3)})_{10}, \quad (6)$$

where the superscripts K (M) refer to KATRIN (Mainz), respectively.

We compare $Q^{\text{calc}} = 18575.72 \pm 0.07$ eV [35] to both $Q^{\text{KATRIN}} = 18575.2 \pm 0.5$ eV [30] and $Q^{\text{Mainz}} = 18576 \pm 3$ eV [38], which was obtained from a dedicated Q value determination campaign of the Mainz experiment. Note that the analysis presented in [18] uses Troitsk data [39] and a different dataset of the Mainz experiment. We find no significant deviation from zero for $(a_{\text{of}}^{(3)})_{10}$ and $(a_{\text{of}}^{(3)})_{00}$ and thus set an upper limit of $|(a_{\text{of}}^{(3)})_{10}| < 6.4 \times 10^{-4}$ GeV and $|(a_{\text{of}}^{(3)})_{00}| < 3.0 \times 10^{-8}$ GeV (90% CL). The limit is dominated by the endpoint uncertainty of the Mainz experiment and thus of similar magnitude than the result obtained in [18].

VI. CONCLUSION

KATRIN is uniquely positioned to study oscillation-free Lorentz-invariance-violating operators that cannot be accessed by time-of-flight or neutrino-oscillation experiments. Based on the first physics run of the KATRIN experiment we were able to probe the parameter $(a_{\text{of}}^{(3)})_{11}$ by searching for a sidereal oscillation of the endpoint of the tritium β -decay spectrum. We find no oscillation and release the first upper limit on this parameter of $|(a_{\text{of}}^{(3)})_{11}| < 0.9 \times 10^{-6} - 3.7 \times 10^{-6}$ GeV (90% CL). Based on the future final KATRIN dataset, a sensitivity at the level of 5×10^{-7} GeV (90% CL) could be reached.

Besides the anisotropic Lorentz-invariance-violating parameter, the parameters $(a_{\text{of}}^{(3)})_{00}$ and $(a_{\text{of}}^{(3)})_{10}$ were investigated using the absolute endpoint measurements of both the KATRIN and the Mainz experiments. We find limits of $|(a_{\text{of}}^{(3)})_{10}| < 6.4 \times 10^{-4}$ GeV and $|(a_{\text{of}}^{(3)})_{00}| < 3.0 \times 10^{-8}$ GeV (90% CL), which is comparable to the limit obtained from Mainz and Troitsk data [18].

This initial study illustrates that the scientific potential of precision β -spectroscopy experiments, such as KATRIN, extends well beyond the neutrino-mass search to physics beyond the standard model.

ACKNOWLEDGMENTS

We acknowledge the support of Helmholtz Association (HGF), Ministry for Education and Research BMBF (No. 05A20PMA, No. 05A20PX3, No. 05A20VK3), Helmholtz Alliance for Astroparticle Physics (HAP), the doctoral school KSETA at KIT, and Helmholtz Young Investigator Group (VH-NG-1055), Max Planck Research Group (MaxPlanck@TUM), and Deutsche Forschungsgemeinschaft DFG (Research Training Groups Grants No. GRK 1694 and No. GRK 2149, Graduate School Grant No. GSC 1085-KSETA, and SFB-1258) in Germany; Ministry of Education, Youth and Sport (CANAM-LM2015056, LTT19005) in the Czech Republic; Ministry of Science and Higher Education of the Russian Federation under Contract No. 075-15-2020-778; and the Department of Energy through Grants No. DE-FG02-97ER41020, No. DE-FG02-94ER40818, No. DE-SC0004036, No. DE-FG02-97ER41033, No. DE-FG02-97ER41041, No. DE-SC0011091, and No. DE-SC0019304 and the Federal Prime Agreement DE-AC02-05CH11231 in the United States. This project has received funding from the European Research Council (ERC) under the European Union Horizon 2020 research and innovation programme (Grant Agreement No. 852845). We thank the computing cluster support at the Max Planck Computing and Data Facility (MPCDF). We would like to thank Ralf Lehnert for fruitful discussions.

-
- [1] V. A. Kostelecký and S. Samuel, *Phys. Rev. D* **39**, 683 (1989).
 - [2] V. A. Kostelecký and R. Potting, *Phys. Rev. D* **51**, 3923 (1995).
 - [3] R. Gambini and J. Pullin, *Phys. Rev. D* **59**, 124021 (1999).
 - [4] S. M. Carroll, J. A. Harvey, V. A. Kostelecký, C. D. Lane, and T. Okamoto, *Phys. Rev. Lett.* **87**, 141601 (2001).
 - [5] D. Colladay and V. A. Kostelecký, *Phys. Rev. D* **55**, 6760 (1997).
 - [6] D. Colladay and V. A. Kostelecký, *Phys. Rev. D* **58**, 116002 (1998).
 - [7] V. A. Kostelecký, *Phys. Rev. D* **69**, 105009 (2004).
 - [8] L. B. Auerbach *et al.*, *Phys. Rev. D* **72**, 076004 (2005).
 - [9] A. A. Aguilar-Arevalo *et al.*, *Phys. Lett. B* **718**, 1303 (2013).
 - [10] Y. Abe *et al.*, *Phys. Rev. D* **86**, 112009 (2012).
 - [11] P. Adamson *et al.*, *Phys. Rev. Lett.* **101**, 151601 (2008).
 - [12] P. Adamson *et al.*, *Phys. Rev. Lett.* **105**, 151601 (2010).
 - [13] P. Adamson *et al.*, *Phys. Rev. D* **85**, 031101 (2012).
 - [14] R. Abbasi *et al.*, *Phys. Rev. D* **82**, 112003 (2010).
 - [15] M. G. Aartsen *et al.*, *Nat. Phys.* **14**, 961 (2018).
 - [16] K. Abe *et al.*, *Phys. Rev. D* **95**, 111101 (2017).
 - [17] D. Adey *et al.*, *Phys. Rev. D* **98**, 092013 (2018).
 - [18] J. S. Díaz, V. A. Kostelecký, and R. Lehnert, *Phys. Rev. D* **88**, 071902 (2013).
 - [19] R. Lehnert, *Phys. Lett. B* **828**, 137017 (2022).
 - [20] J. Angrik *et al.*, KATRIN design report, Technical Report No. 7090, FZKA, 2005.
 - [21] M. Aker *et al.*, *J. Instrum.* **16**, T08015 (2021).
 - [22] M. Aker *et al.*, *Nat. Phys.* **18**, 160 (2022).
 - [23] V. Lobashev and P. Spivak, *Nucl. Instrum. Methods Phys. Res., Sect. A* **240**, 305 (1985).
 - [24] A. Picard, H. Backe, H. Barth, J. Bonn *et al.*, *Nucl. Instrum. Methods Phys. Res., Sect. B* **63**, 345 (1992).
 - [25] F. Priester, M. Sturm, and B. Bornschein, *Vacuum* **116**, 42 (2015).
 - [26] M. Arenz *et al.*, *J. Instrum.* **2018**, T08005 (2018).
 - [27] A. Marsteller *et al.*, *Vacuum* **184**, 109979 (2021).
 - [28] M. Arenz, W. J. Baek, M. Beck, A. Beglarian, J. Behrens, T. Bergmann, A. Berlev, U. Besserer, K. Blaum, T. Bode, B. Bornschein, L. Bornschein *et al.*, *Eur. Phys. J. C* **78**, 368 (2018).
 - [29] J. F. Amsbaugh *et al.*, *Nucl. Instrum. Methods Phys. Res., Sect. A* **778**, 40 (2015).
 - [30] M. Aker *et al.*, *Phys. Rev. Lett.* **123**, 221802 (2019).
 - [31] M. Aker *et al.*, *Phys. Rev. D* **104**, 012005 (2021).
 - [32] M. Kleesiek *et al.*, *Eur. Phys. J. C* **79**, 204 (2019).
 - [33] S. Mertens *et al.*, *Astropart. Phys.* **41**, 52 (2013).
 - [34] S. S. Wilks, *Ann. Math. Stat.* **9**, 60 (1938).

-
- [35] E. G. Myers, A. Wagner, H. Kracke, and B. A. Wesson, *Phys. Rev. Lett.* **114**, 013003 (2015).
- [36] E. W. Ottenand and C. Weinheimer, *Rep. Prog. Phys.* **71**, 086201 (2008).
- [37] C. Kraus, B. Bornschein, L. Bornschein *et al.*, *Eur. Phys. J. C* **40**, 447 (2005).
- [38] C. Weinheimer *et al.*, *Phys. Lett. B* **300**, 210 (1993).
- [39] V. N. Aseev *et al.*, *Phys. Rev. D* **84**, 112003 (2011).